Applied Catalysis B: Environmental 174–175 (2015) 136–144

Contents lists available at ScienceDirect

Applied Catalysis B: Environmental

journal homepage: www.elsevier.com/locate/apcatb

Oxidation of ammonia using PtRh/C electrocatalysts: Fuel cell and electrochemical evaluation

Mônica H.M.T. Assumpção[a], Ricardo M. Piasentin[a], Peter Hammer[b], Rodrigo F.B. De Souza[a], Guilherme S. Buzzo[a], Mauro C. Santos[c], Estevam V. Spinacé[a], Almir O. Neto[a], Júlio César M. Silva[a,*]

[a] Instituto de Pesquisas Energéticas e Nucleares, IPEN/CNEN-SP, Av. Prof. Lineu Prestes, 2242 Cidade Universitária, CEP 05508-900 São Paulo, SP, Brazil
[b] Instituto de Química, UNESP – Universidade do Estado de São Paulo, 14801-970 Araraquara, SP, Brazil
[c] Laboratório de Eletroquímica e Materiais Nanoestruturados, Centro de Ciências Naturais e Humanas, Universidade Federal do ABC, Rua Santa Adélia, 166, CEP 09210-170 Santo André, SP, Brazil

ARTICLE INFO

Article history:
Received 26 November 2014
Received in revised form 4 February 2015
Accepted 17 February 2015
Available online 20 February 2015

Keywords:
Direct ammonia fuel cell
PtRh/C catalysts
Borohydride reduction methods

ABSTRACT

This study reports on the use of PtRh/C electrocatalysts prepared by the borohydride reduction method with different Pt:Rh atomic ratios: (90:10, 70:30 and 50:50) which was investigated toward the ammonia electro-oxidation considering electrochemical and also direct ammonia fuel cell (DAFC) experiments. The DAFC experiments were conducted using different proportions of NH_4OH and KOH as fuels. X-ray diffraction showed the formation of PtRh alloy while transmission electron micrographs showed the particles sizes between 4.1 and 4.5 nm. Among the different NH_4OH and KOH concentrations the combination of 3 mol L^{-1} NH_4OH and 3 mol L^{-1} KOH was the most favorable due to the higher KOH concentration, which increased the electrolyte conductivity, thus, improving the ammonia oxidation. Moreover, among the PtRh/C electrocatalysts the Pt:Rh ratio of 90:10 showed to be the best suited one since it showed a power density almost 60% higher than Pt. X-ray photoelectron spectroscopy results revealed for this catalyst that the nanoparticles contain a high proportion of metallic Pt and Rh phases, supporting the alloy formation between Pt and Rh. The improved fuel cell efficiency can be related to the combination of different effects: the alloy formation between Pt and Rh (electronic effect), suppressing the adsorption strength of poisonous intermediates, and a synergic effect between Pt and Rh at this composition.

1. Introduction

The use of excessive fossil fuels, principally in the transportation sectors, has resulted in harmful effects on human health and also to the environment. Therefore, there is a strong need to come up with some environmentally benign and sustainable alternatives [1]. Considering these aspects and taking into account that the most used fuel in fuel cells is hydrogen, fuel cells represent a promising alternative and if widely implemented in transport and stationary power generation, they could significantly contribute to reduction of greenhouse gas emissions [2,3].

However, several technological challenges related to hydrogen transportation and storage infrastructure have yet to be solved [2,4]. Thus, the use of alternative fuels such as ammonia has been receiving a growing attention due to its low cost, stability and eases of storage [5]. Furthermore, ammonia is a CO free fuel and in terms of energy density, only ammonia and hydrides exhibit an energy density close to fossil fuels such as coal and oil, much higher than compressed hydrogen [5–7].

Indeed, the theoretical specific charge of complete ammonia oxidation to N_2 is 4.75 Ah g^{-1}, that is 95% of the charge of methanol oxidation to CO_2 [8]. Moreover, ammonia is also one of the most concerning industrial wastes because of its large-scale production and being the second largest chemical produced all over the world [9,10].

Thus, in order to use ammonia as a fuel and also to improve the kinetics of ammonia oxidation reaction at low temperatures, different catalysts were already suggested such as PtIr, PtNi, PdIr, PtPd, PdNi and others. However, until now the Pt group metals show the most promising catalytic activity toward this reaction [8,11–16].

Actually, the commonly used electrode for ammonia oxidation is Pt, however, some reaction intermediates and adsorbed species also lead to the deactivation of platinum during this reaction. Normally, the formation of N_{ads} causes the poisoning of the Pt surface

* Corresponding author. Tel.: +55 11 3133 9284; fax: +55 11 3133 9285.
E-mail address: quimijulio@gmail.com (J.C.M. Silva).

http://dx.doi.org/10.1016/j.apcatb.2015.02.021
0926-3373/

because the adsorption energy of N_{ads} on Pt is relatively high [17]. Then, in order to improve Pt electrocatalytic performance of ammonia oxidation the use of platinum-based binary catalysts is an attractive alternative [8,11–15].

In the Pt binary nanoparticles, Pt is more employed not only because of its electrocatalytic properties but also due to the fact that N_{ads} is formed at very high potentials [18] and among the metals suggested to be active toward the ammonia oxidation Rh is reported as a promising candidate [19,20]. Hung [19] proposed that rhodium-based metal improves the nitrogen oxide conversion properties of the catalysts and the selectivity toward dinitrogen, what could contribute to the ammonia oxidation.

Aiming the development of direct ammonia fuel cells (DAFCs) the present study describes the use of different PtRh/C electrocatalysts with different Pt:Rh atomic ratios (50:50, 70:30 and 90:10) to be used as anode electrocatalysts of a DAFC. In this study, it was also evaluated the influence of NH_4OH and KOH concentrations used as fuels. Additionally, electrochemical experiments were performed in order to obtain more information about the materials toward ammonia electro-oxidation.

2. Experimental

PtRh/C electrocatalyts (20 wt% of metals loading) with different atomic ratios: 50:50, 70:30 and 90:10, Rh/C and Pt/C, were prepared by the borohydride reduction process [21,22] using $H_2PtCl_6{\cdot}6H_2O$ (Aldrich) and $Rh(H_2O)(OH)_{3-y}(NO3)_y$ (Aldrich), as metal sources. All catalysts were supported on carbon (Vulcan XC 72). The electrocatalysts were firstly characterized by X-ray diffraction (XRD) using a Rigaku diffractometer model Miniflex II using Cu Kα radiation source (0.15406 nm), being the X-ray diffraction patterns recorded in the range of $2\theta = 20^\circ$–90° with a step size of 0.05° and a scan time of 2 s per step. Transmission electron microscopy (TEM) images were also carried out using a JEOL transmission electron microscope model JEM-2100 operated at 200 kV. The atomic ratios of Pt and Rh in the synthesized materials were measured by energy dispersive spectroscopy (EDS) by using a JEOL–JSM6010 LA equipment.

The XPS analysis was carried out at a pressure of less than 10^{-7} Pa using a commercial spectrometer (UNI-SPECS UHV). The MgKα line was used ($h\nu = 1253.6$ eV) and the analyzer pass energy was set to 10 eV. The inelastic background of the Pt 4f, Rh 3p, C 1s and O 1s electron core-level spectra was subtracted using Shirley's method. The composition (at.%) of the near surface region was determined with an accuracy of ±5% from the ratio of the relative peak areas corrected by Scofield's sensitivity factors of the corresponding elements. The spectra were fitted without placing constraints using multiple Voigt profiles. The width at half maximum (FWHM) varied between 1.0 and 2.2 eV and the accuracy of the peak positions was ±0.1 eV.

Electrochemical measurements were performed at room temperature using a potentiostat/galvanostat PGSTAT 302N Autolab, using a conventional three-electrode electrochemical cell. A platinum electrode and a Hg/HgO were used as the counter and reference electrodes, respectively. Glassy carbon (GC) electrodes were employed as support for the working electrodes (0.166 cm^2 of geometric area). Before each experiment, the GC support was polished with alumina suspension (1 μm) and washed in water. Ultrapure water obtained from a Milli-Q system (Millipore®) was used in all experimental procedures.

The working electrodes were constructed by dispersing 8 mg of the electrocatalyst powder in 1 mL water and mixing for 15 min in an ultrasonic bath. Shortly thereafter, 20 μL of 5% Nafion® solution was added to the suspension, which was mixed again for 20 min in an ultrasonic bath. Aliquots of 16 μL of the dispersion fluid were pipetted onto the GC surface, leading to a metal loading of 151 μg of metal/cm^2. Finally, the electrode was dried at 60 °C for 20 min and hydrated for 2 min in water. All the electrochemical measurements were performed in a 1 mol L^{-1} KOH solution.

Cyclic voltammograms (CV) were carried out at a scan rate of 20 mV s^{-1} between −0.85 V and 0.2 V *vs* Hg/HgO. The electrocatalysts were cycled for five consecutive cycles resulting in the stable and reproducible shape of the voltammogram in ammonia free solutions and three consecutive cycles in ammonia containing solutions. Chronoamperometric experiments were carried out for 2 h at −0.30 V *vs* Hg/HgO. The electro-oxidation of ammonia was performed in a 1 mol L^{-1} KOH and 1 mol L^{-1} NH_4OH solution.

DAFCs experiments were conducted as already described by our research group [13,24]. In these experiments a single cell with 5 cm^2 of area were employed being the temperature of it set to 50 °C and 85 °C for the oxygen humidifier. All electrodes were constructed with 2 mg of metal per cm^2 in the anode or in the cathode. For all experiments a commercial Pt/C (BASF) was used as cathode. A Nafion® 117 membrane previously exposed to 6 mol L^{-1} KOH for 24 h [13,25] was also used for these experiments.

In order to evaluate which fuel is more efficient in the DAFCs we studied several combinations of KOH and NH_4OH concentrations as fuels: KOH ranging from 0.0 mol L^{-1} to 3.0 mol L^{-1} and NH_4OH ranging from 1.0 mol L^{-1} to 5.0 mol L^{-1}. The fuels were delivered at 1 mL min^{-1}, and the oxygen flow was regulated at 150 mL min^{-1}. Polarization curves were obtained by using a potentiostat/galvanostat PGSTAT 302N Autolab.

Table 1
PtRh lattice parameter, a, and mean grain diameter, d, sizes obtained by XRD and by TEM images.

Pt:Rh	XRD parameters (nm)						TEM
	a (Pt)	d (Pt)	a (PtRh)	d (PtRh)	a (Rh)	d (Rh)	d (nm)
100:0	0.392	5	–	–	–	–	–
90:10	0.392	5	0.387	9	0.382	9	4.1
70:30	0.392	6	0.386	6	0.381	8	4.5
50:50	0.392	6	0.386	6	0.381	6	4.2
0:100	–	–	–	–	0.381	4	4.1

3. Results and discussion

Fig. 1 shows the XRD patterns of the synthesized Pt/C, Rh/C and PtRh/C with different compositions, all prepared by the borohydride reduction process. The XRD patterns show five main peaks of the face-centered cubic (fcc) crystalline structure of Pt and Rh, namely the (1 1 1), (2 0 0), (2 2 0), (3 1 1) and (2 2 0) planes [26], accordingly to JCPDF # 04 802 and JCPDF # 88 2334, respectively. A broad peak at 2θ about 25° was also observed and assigned to the (0 2 2) reflection of the hexagonal structure of Vulcan XC 72 carbon [27,28].

With increasing Rh content, the PtRh/C electrocatalysts showed diffractograms with peaks shifting to higher 2θ values when compared to Pt/C. The observed shift indicates a lattice constriction due to the incorporation of smaller Rh atoms into the Pt fcc structure, suggesting the alloy formation of Pt–Rh. In order to confirm the alloy formation, the 2 2 0 crystal planes were deconvoluted and the lattice parameters were calculated for all synthesized materials, as already reported on the literature [29,30]. The red line is assigned to the Pt and green line to the Rh. The lattice parameter, listed in Table 1, have shown for all PtRh/C electrocatalysts values lower than that of Pt, supporting the formation of an alloyed phase. The formation of PtRh alloy has been also suggested by other authors [31–33].

The experimental compositions of all PtRh/C materials using the EDS analysis were 91:9 (nominal 90:10), 75:25 (nominal 70:30),

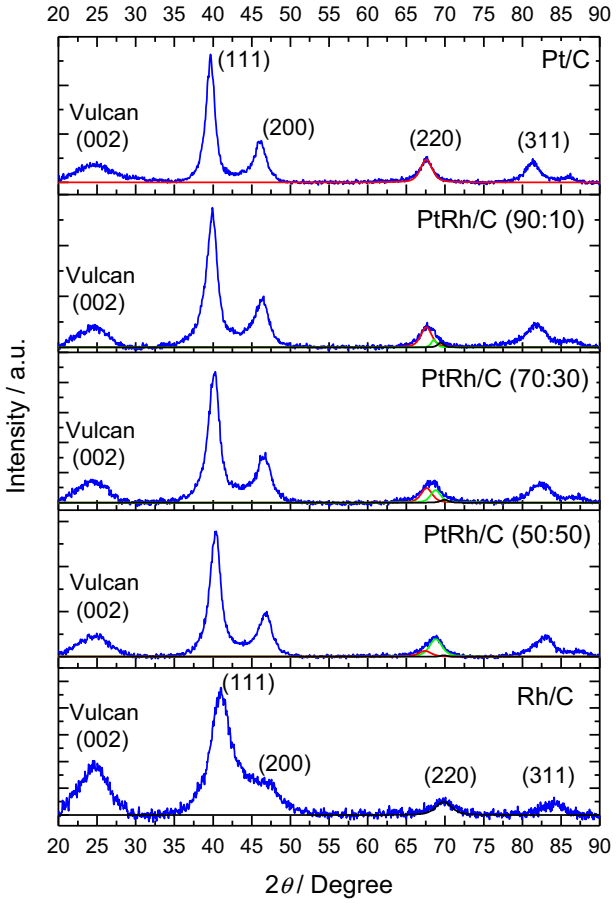

Fig. 1. X-ray diffraction patterns for the Pt/C, PtRh/C and Rh/C electrocatalysts.

61:39 (nominal 50:50). As can be seen, the real atomic ratios of each PtRh/C catalysts are close to nominal values in all cases. Also, in quantitative XPS analysis for two binary PtRh/C samples, the nominal Pt to Rh ratios of the near surface region were: 91.5:9.5 (nominal 90:10) and 45.5:54.5 (nominal 50:50), determined with and error of ±10%.

Fig. 2 shows TEM micrographs and histograms of the particle mean diameter distribution for the binary PtRh/C and Rh/C catalysts. In all images the particles were well dispersed on carbon support, although some small particle agglomerations can also be observed. The mean average size was determined by counting about 200 particles at different regions of the different electrocatalysts. The mean diameter of the nanoparticles is also showed on Table 1. It is important to stress that the borohydride method yields a narrow size distribution, characteristic of this method of preparation [34].

To obtain information of the bonding state of the catalysts XPS high-resolution Pt 4f, Rh 3d and O1s core level spectra were recorded. As shown in Fig. 3, the deconvoluted Pt 4f spectrum are formed by four spin-orbit doublets with binding energies of Pt $4f_{7/2}$ components at 71.3 eV, 72.0 eV, 73.5 eV and 74.4 eV, attributed to metallic Pt, $Pt(OH)_2$, PtO and PtO_2 phases, respectively [35]. As the mean particle size is smaller than the XPS sampling depth (~5 nm) the XPS data reflect the core–shell structure of the catalyst, with a near surface region formed by an internal layer of PtO followed by external layers of PtO_2 and $Pt(OH)_2$. Considering the fitted peak areas of the Pt/C catalyst it can be observed in Fig. 3 that the hydroxide/oxide layers (74.6% of the peak area) form the major part of the Pt nanoparticles. In contrast, for the PtRh/C (90:10) and PtRh/C (50:50) electrode the contribution of these layers is only about 54% and 63%, respectively, indicating the predominance of the metallic Pt phase of the PtRh/C (90:10).

The Rh $3d_{3/2}$ spectra, shown in Fig. 4, were fitted with three components, centered at 307.3 eV, 308.2 eV and at about 310 eV, assigned to metallic Rh, Rh_2O_3, and RhC_xN_y phases, respectively [35]. In analogy to oxides/hydroxides, detected for platinum, the latter Rh phases are expected to form the surface region of the nanoparticles. The corresponding Pt and Rh oxide components were identified in the O 1s spectra at 530, 5 eV (not shown). Fierro et al. [36] reported for the PtRh/C (90:10) phase binding energies of 71.1 eV for Pt $4f_{7/2}$ and 309.4 eV for Rh $3d_{5/2}$. Therefore, it cannot be excluded that the Rh $3d_{5/2}$ component close to 310 eV could be related to PtRh alloy. In the case of platinum the 71.1 eV peak position overlaps with the Pt $4f_{7/2}$ component of the metallic phase. Although the Rh 3d spectrum (Fig. 4), recorded for the PtRh/C (90:10) catalyst, is quite noisy and the high-energy part superimposed by a strong Pt $4d_{5/2}$ signal, the sub-peak intensities allow to compare the contribution of each Rh phase for three Rh containing catalysts. The result shows that the PtRh/C (90:10) catalyst has the highest proportion of metallic phase (~60%), while for the PtRh/C (50:50) and Rh/C catalyst only 48.7% and 39.5% Rh^0 was determined, respectively. The combination of results obtained from the Pt 4f and Rh 3d peak-fitting analysis indicates that the PtRh/C (90:10) catalyst is formed mainly by metallic Pt and Rh phases, possibly forming an alloy, which should favor the ammonia oxidation reaction.

The cyclic voltammograms in 1 mol L^{-1} KOH of Pt/C and PtRh/C (90:10, 70:30, 50:50) electrocatalysts between −0.85 V and 0.2 V are shown in Fig. 5. For Pt/C the hydrogen adsorption/desorption region is located in potential of −0.8 V to −0.4 V [37]. The peak

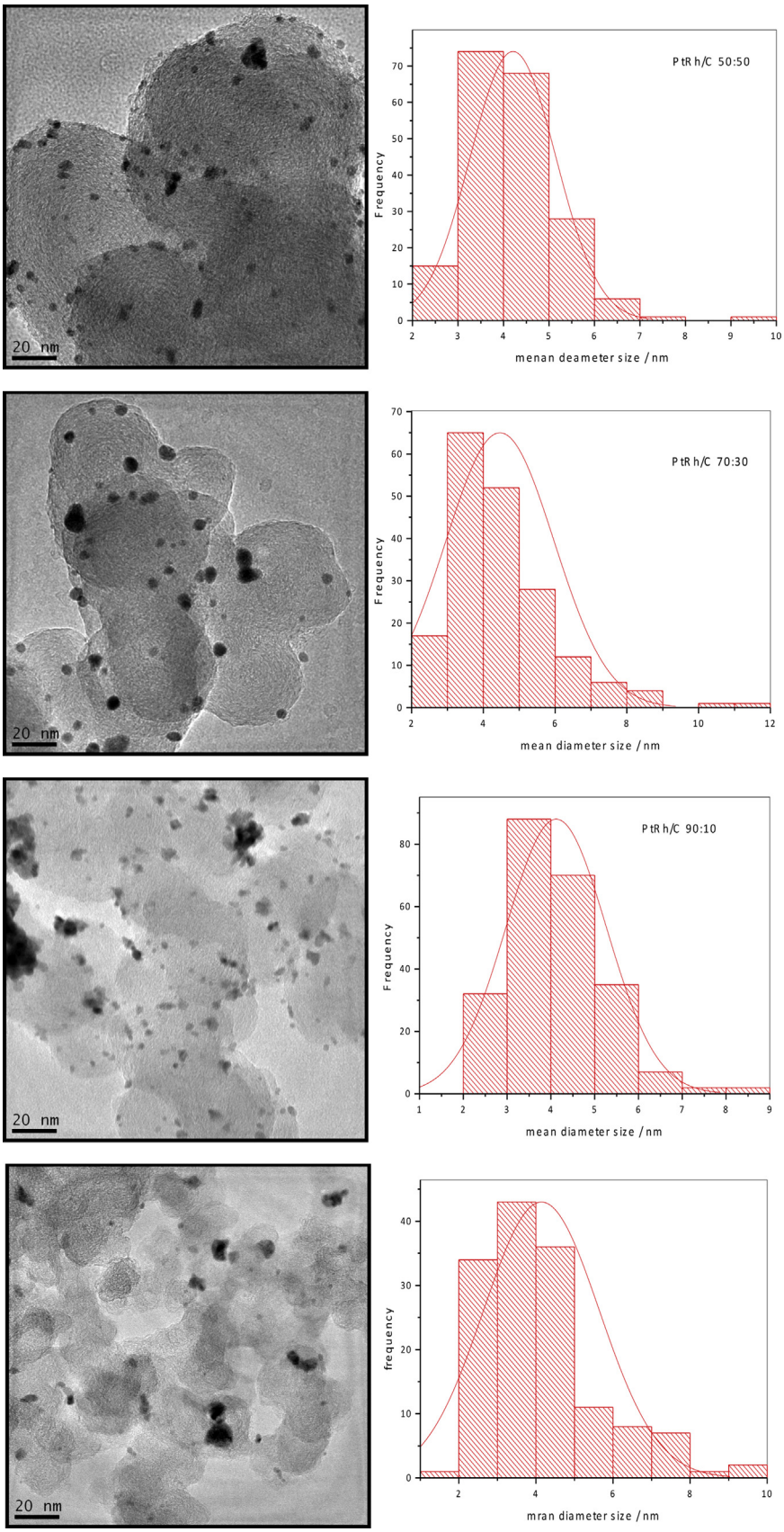

Fig. 2. TEM micrographs and histograms of (a) PtRh/C 90:10, (b) PtRh/C 70:30, (c) PtRh/C 50:50 and (d) Rh/C.

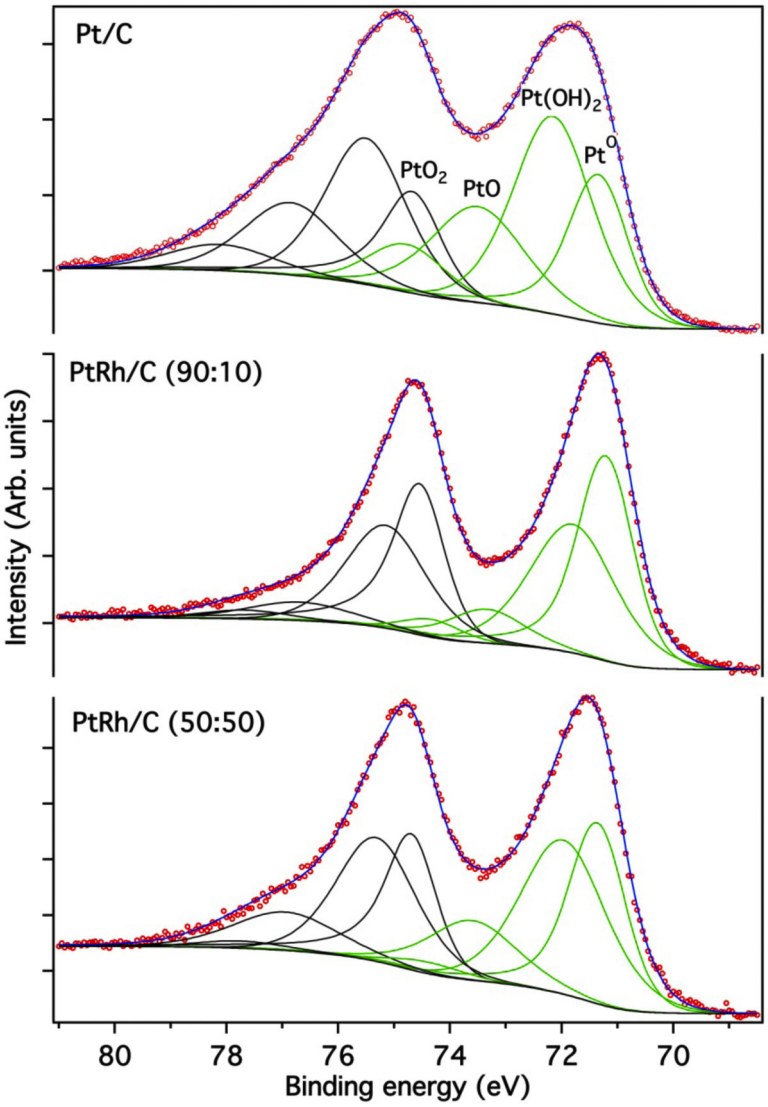

Fig. 3. Fitted XPS Pt 4f core level spectra of the Pt/C, PtRh/C 90:10, PtRh/C 50:50 catalyst.

around −0.11 V on the positive scan is related to the adsorption of OH on the catalyst surface and the potential region from −0.20 to 0.2 V is associated to the formation of an oxide layer on the platinum surface [38]. In the reversible scan the peak at about −0.18 V is related to the reduction of oxides [39]. For PtRh/C binary materials is possible to observe that the hydrogen desorption/adsorption and the OH adsorption peaks decreases as the Rh amount in the materials increases, indicating that the Rh are blocking the Pt surface. These results are in agreement with XPS analyzes that shown more oxides species on the PtRh/C 50:50 than on PtRh/C 90:10 surfaces. The changes on Pt profile obtained from CV in alkaline media were also reported in the literature using PtSn/C [38].

Fig. 6 shows the cyclic voltammograms of Pt/C and PtRh/C (90:10, 70:30, 50:50) electrocatalysts in 1 mol L^{-1} KOH + 1 mol L^{-1} NH_4OH. It is possible to observe that the onset potential for ammonia electro-oxidation on Pt/C is in higher values than the ones obtained using PtRh/C binary materials, this results are in agreement with the literature [18,40]. An important observation is that the lowest value of onset potential (∼−0.54 V) for ammonia electro-oxidation was obtained using PtRh/C 50:50 as electrocatalyst. Considering the ammonia oxidation on PtRh electrocatalysts, Vidal-Iglesias et al. [18] showed that in some catalysts based on PtRh the onset potential shifts toward lower potentials producing higher current densities than on pure Pt. Hung [19] suggested that rhodium-based alloys improve the nitrogen oxide conversion of the catalysts and the selectivity toward dinitrogen. Additionally, Vooys et al. [20] reported that Rh dehydrogenate the ammonia molecule at significantly lower potentials than on Pt and Ir. Moreover, the adsorption energy of atomic N_{ads} on Rh is considerably higher than on Pt [20], what could explain the decrease in ammonia oxidation as the Rh atomic ratio increases in the catalysts.

Taking into account the peak current density for ammonia electro-oxidation, the highest value was obtained using PtRh/C 90:10, indicating that introducing small amounts of Rh in Pt electrocatalysts it is possible to improve the ammonia electro-oxidation. Then the use of Rh in the binary PtRh catalyst can contribute to the ammonia oxidation reaction.

Fig. 7 shows the chronoamperometric curves for 1 mol L^{-1} NH_4OH + 1 mol L^{-1} KOH electro-oxidation on Pt/C and PtRh/C (90:10, 70:30, 50:50) electrocatalysts, obtained by polarization at −0.30 V for 120 min. Using PtRh/C 90:10 as electrocatalyst, the current density associated to the ammonia electro-oxidation was higher than that obtained using other catalysts. Pt/C and PtRh/C 50:50 deactivates in about 25 min and 40 min, respectively. Lomocso and Baranova [15] also observe the Pt/C deactivation in less than 60 min using 1 mol L^{-1} KOH and 0,5 mol L^{-1} NH_4OH. The

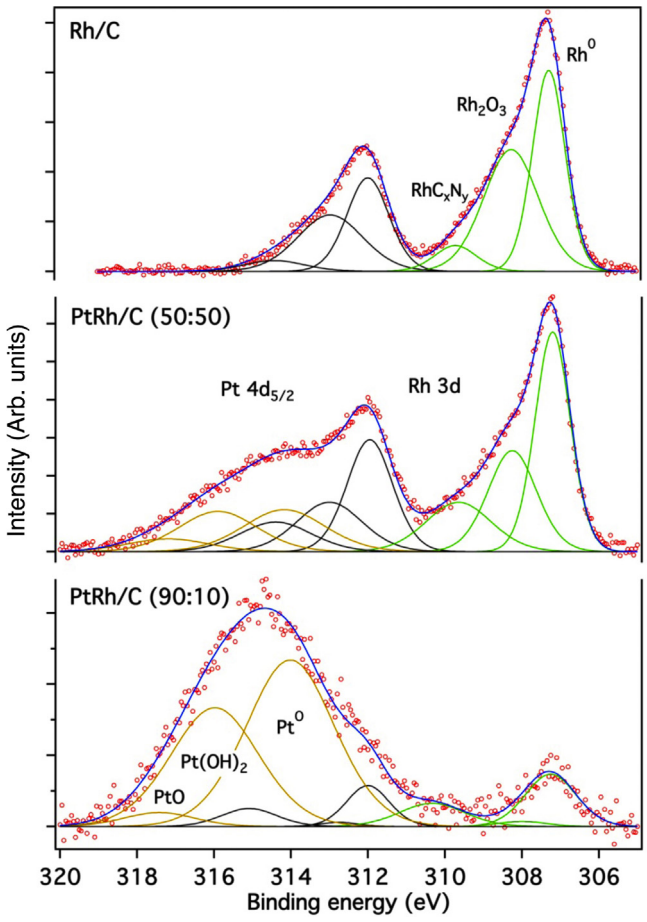

Fig. 4. Fitted XPS Rh 3d core level spectra of the Rh/C, PtRh/C 50:50, PtRh/C 90:10 catalyst. (In the presence of Pt the Rh $3d_{3/2}$ spin orbit components overlap with the Pt $4d_{5/2}$ intensities).

PtRh/C 50:50 deactivation might be related to the poisoning on the catalyst surface by N_{ads} due to the higher amount of Rh in this proportion. The best result obtained using PtRh/C 90:10 could be related to the predominant metallic phase as shown in the XPS analyzes. Similar results were obtained by Allagui et al. [8] using PtIr/C synthesized in different pH values. The authors reported that the

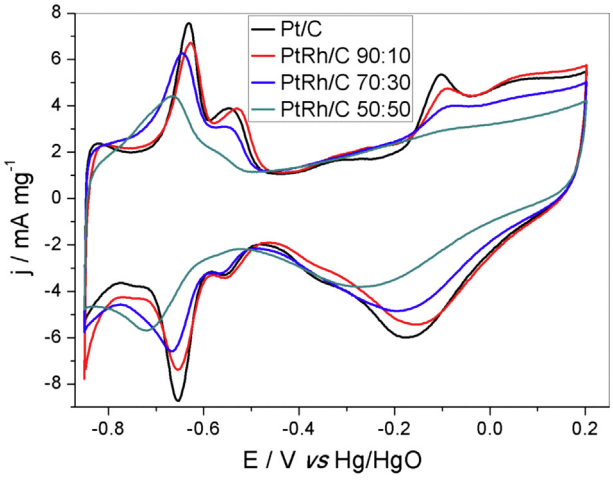

Fig. 5. Cyclic voltammograms of Pt/C and PtRh/C electrocatalysts in 1 mol L^{-1} KOH at $\nu = 20$ mV s^{-1} at room temperature.

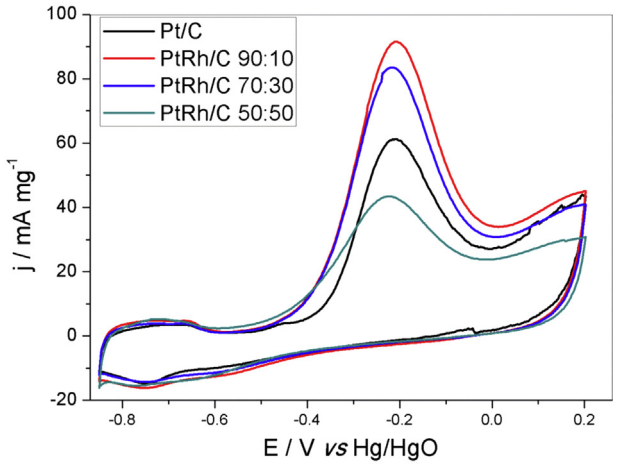

Fig. 6. Cyclic voltammograms of Pt/C and PtRh/C electrocatalysts in 1 mol L^{-1} KOH + 1 mol L^{-1} NH_4OH at $\nu = 20$ mV s^{-1} at room temperature.

material with the lowest amount of oxide on the surface shows higher catalytic activity toward ammonia electro-oxidation.

Considering DAFC experiments, it is known that Nafion® membrane exhibits excellent balance of high chemical, electrochemical and thermal stability, and also high proton conductivity [25]. Furthermore, due to its better endurance in alkaline solution, it is also used as electrolyte in chlorine-alkali industry and alkaline direct borohydride fuel cell [41]. Considering alkaline direct ethanol fuel cell just few authors reported on alkali modified Nafion® membrane and among them NaOH is usually used to modify Nafion® [42], although it is well known that KOH solution has higher ionic conductivity than NaOH under the same conditions.

Hou et al. [25] studied the ionic conductivity of Nafion 112/KOH membranes for different KOH concentrations: 1 mol L^{-1}, 3 mol L^{-1} and 6 mol L^{-1}. The corresponding ionic conductivity was 0.011 S cm^{-1}, 0.026 S cm^{-1} and 0.032 S cm^{-1}, respectively, evidencing that the ionic conductivity of Nafion® 112 membrane increases with the KOH concentration. Consequently, the highest power density is expected to be observed at the higher KOH concentrations.

In order to study more deeply the fuel influence in the fuel cell performance we evaluated in DAFCs experiments different combinations of NH_4OH and KOH concentrations.

Fig. 8 displays cell voltage and power density as a function of the current density obtained for 1 mol L^{-1} NH_4OH, varying the KOH concentration between 0 mol L^{-1} and 3 mol L^{-1}. Fig. 9 shows the

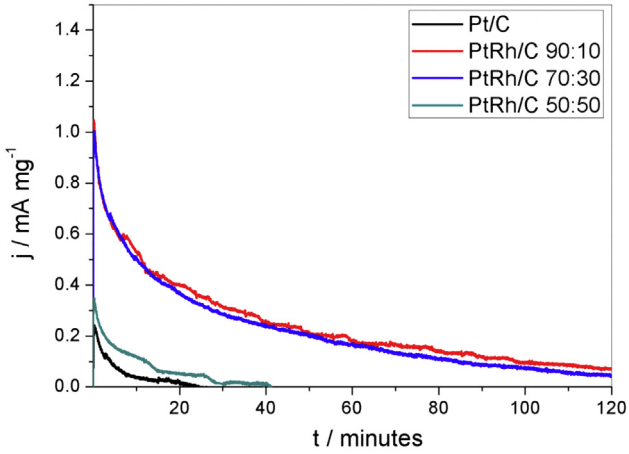

Fig. 7. Chronoamperometric measurements at −0.30 V *vs* Hg/HgO for Pt/C and PtRh/C electrocatalysts in 1 mol L^{-1} KOH + 1 mol L^{-1} NH_4OH at room temperature.

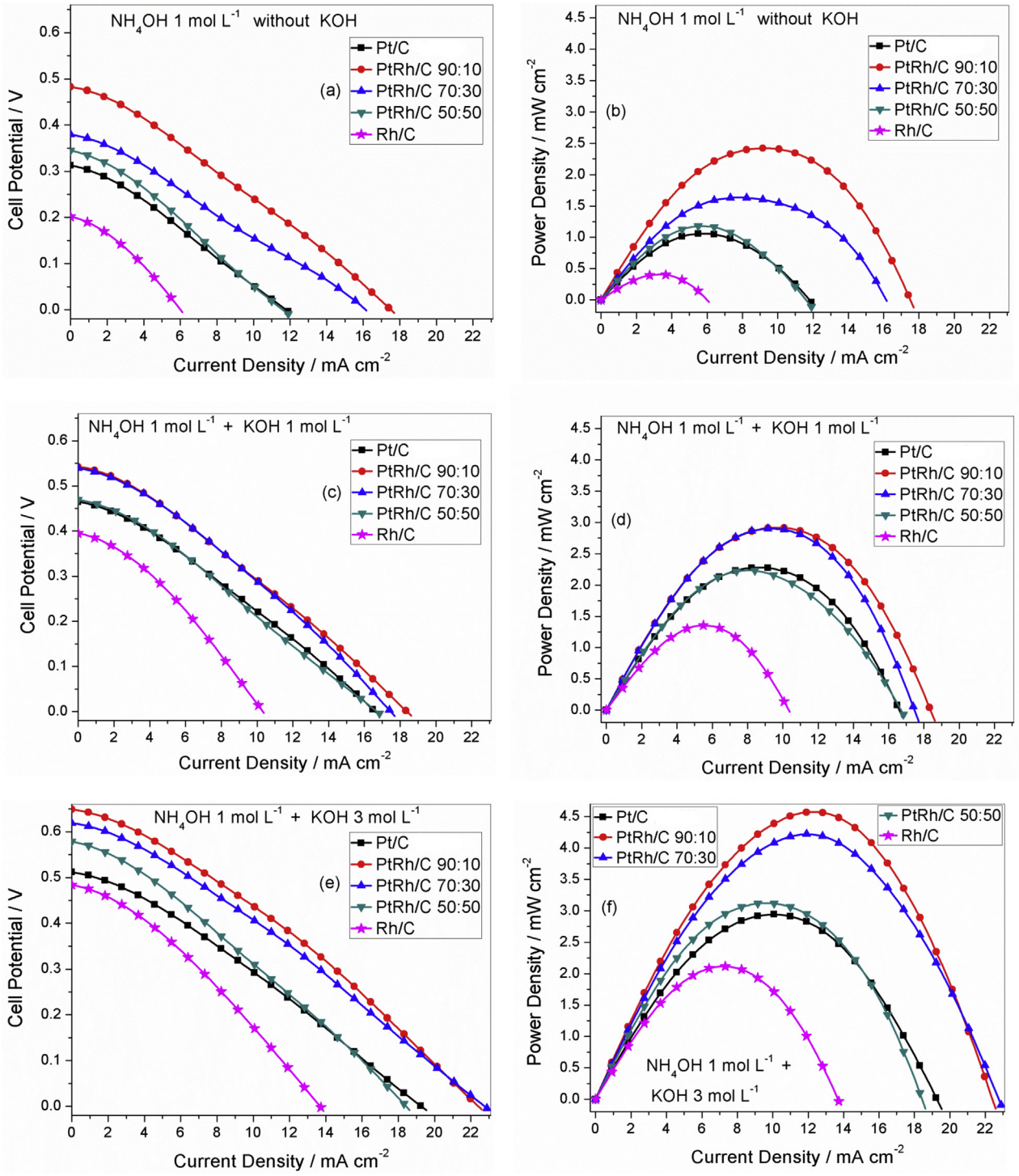

Fig. 8. Polarization and power density curves of a 5 cm^2 DAFC with 2 mg metal cm^{-2} in both anode and cathode at 50 °C and using 1 mol L^{-1} NH_4OH and KOH ranging from 0 mol L^{-1} to 3 mol L^{-1}.

maximum power density *vs* atomic composition of Pt in PtRh/C electrocatalysts, using 1 mol L^{-1}, 3 mol L^{-1} and 5 mol L^{-1} NH_4OH, varying for each NH_4OH value, the KOH concentration between 0 mol L^{-1} and 3 mol L^{-1}.

The results, summarized in Tables 2 and 3, show that increasing the KOH concentration there is also an increase of the cell potential and power density, showing best performance for all studied catalyst at 3 mol L^{-1} NH_4OH and 3 mol L^{-1} KOH. The fuel cell performance (maximum power density) was about twice higher using 3 mol L^{-1} KOH, compared to the fuel cell performance without KOH for all NH_4OH concentrations. In all experiments, the highest cell potential and power density were obtained for Pt:Rh ratio of 90:10, followed by catalysts with ratios of 70:30, 50:50, 100:0 and 0:100.

Analyzing the KOH concentration dependence it is possible to affirm that there was an increase in the conductivity induced by higher KOH concentration leading to a higher power density. Similar results of increased activity at elevated KOH concentrations was reported by Yao and Cheng [11] using Ni–Pt anodes.

Recent studies using PtIr anodes [13] showed that the increase of the NH_4OH concentration results in an significant improvement

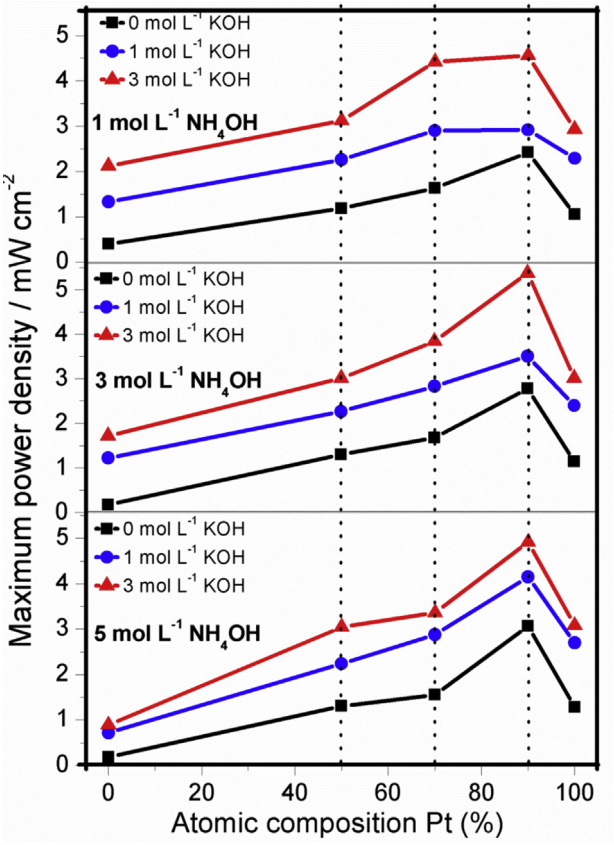

Fig. 9. Maximum power density *vs* atomic composition of Pt in PtRh/C electrocatalysts using 1 mol L^{-1}, 3 mol L^{-1}, 5 mol L^{-1} NH_4OH and KOH ranging from 0 mol L^{-1} to 3 mol L^{-1}.

of the power density. Allagui et al. [43] studied different ammonia concentrations using PdNi electrocatalysts and observed a linear increase of the ammonia oxidation when increasing its concentration, followed by a slight activity decrease at higher concentrations. They related the saturation behavior to the lack of active species on the catalyst surface available for the ammonia oxidation. On the other hand, Lomocso and Baranova [15] attributed the decrease of maximum peak current density at higher NH_4OH concentrations to the increasing in the N_{ads} formation, blocking active sites and preventing ammonia electro-oxidation. Additionally, the electrode surface could be also saturated with other adsorbed species, affecting the capability of the catalysts to oxidize at higher ammonia concentrations [15].

Recently, we investigated the DAFC performance of Pd/C, PdIr/C and Ir/C as anode electrocatalysts [24], observing that for Pd/C and PdIr/C (90:10) both OCV and maximum power density were lower using 5 mol L^{-1} than 3 mol L^{-1} NH_4OH. This was attributed to the increased rate of N_{ads} formation at 5 mol L^{-1} NH_4OH, blocking actives sites since ammonia dehydrogenation on Pd occurs at low potential favoring the formation of the poisonous N_{ads} species.

The low DAFC performance of the Rh/C catalyst at 5 mol L^{-1} NH_4OH, observed in the present work, suggests that at high NH_4OH concentrations the formation rate of N_{ads} increases on Rh electrode, since the ammonia is dehydrogenated in significant lower potential on Rh than on Pt [44]. Additionally, the adsorption energy of

Table 2
Open circuit potential (OCV) obtained during DAFC experiments at 50 °C.

NH_4OH concentrations (mol L^{-1})	KOH concentrations (mol L^{-1})	Electrocatalysts compositions Pt:Rh				
		100:0	90:10	70:30	50:50	0:100
		OCV/V				
1.0	0.0	0.31	0.48	0.38	0.35	0.20
	1.0	0.46	0.54	0.54	0.47	0.39
	3.0	0.51	0.65	0.62	0.58	0.48
3.0	0.0	0.32	0.50	0.37	0.35	0.12
	1.0	0.46	0.57	0.52	0.47	0.36
	3.0	0.51	0.68	0.58	0.54	0.41
5.0	0.0	0.33	0.52	0.36	0.34	0.12
	1.0	0.47	0.62	0.50	0.46	0.26
	3.0	0.51	0.64	0.53	0.51	0.28

Table 3
Maximum power density (MPD) obtained during DAFC experiments at 50 °C.

NH_4OH concentrations (mol L^{-1})	KOH concentrations (mol L^{-1})	Electrocatalysts compositions Pt:Rh				
		100:0	90:10	70:30	50:50	0:100
		MPD/mWcm^{-2} align=ĉenter¨				
1.0	0.0	1.05	2.42	1.63	1.18	0.40
	1.0	2.29	2.92	2.90	2.26	1.33
	3.0	2.93	4.56	4.22	3.12	2.12
3.0	0.0	1.14	2.78	1.68	1.30	0.17
	1.0	2.40	3.51	2.83	2.27	1.22
	3.0	3.02	5.37	3.84	3.02	1.72
5.0	0.0	1.28	3.07	1.56	1.31	0.19
	1.0	2.70	4.15	2.88	2.24	0.72
	3.0	3.08	4.92	3.36	3.05	0.89

atomic N_{ads} on Rh ($-448\,kJ\,mol^{-1}$) is considerably higher than on Pt ($-394\,kJ\,mol^{-1}$) [20], which could explain the decrease in the maximum power density as the Rh atomic ratio increases in the catalysts.

In this context the formation of a PtRh alloy, indicated by the XRD data, could have a synergetic effect to the ammonia oxidation since the electronic effect of the valence band structure might contribute to the reduction of the adsorption strength of poisonous intermediates. Furthermore, among all the electrocatalysts in this study, the PtRh/C (90:10) showed to be the most promising material since the power density, obtained in a DAFC, was almost 60% higher than that obtained using Pt/C as anode at $3\,mol\,L^{-1}$ NH_4OH and $3\,mol\,L^{-1}$ KOH. This result could also be explained by a synergic effect of Pt and Rh, which combines the dehydrogenation ammonia at lower over potential at Rh sites with low adsorption energy of N_{ads} on Pt (compared to Rh) [20]. This behavior can be explained by the favorable effect of the electronic structure of the metallic phase (valence band orbitals), found by XPS to be the predominant phase in the PtRh/C (90:10). Comparing the overall performance of the PtRh/C (90:10) catalyst with previous results, it is important to point out that the power density obtained for the PtRh/C (90:10) was higher than that found in previous studies using PtIr/C catalysts [13] and PdIr/C [24]. Also the OCV values were higher than those obtained by Suzuki et al. [45] using PtRu/C as anode, although at different conditions.

4. Conclusions

Results obtained from direct ammonia fuel cells experiments, using different combinations of NH_4OH and KOH concentrations, clearly showed that the KOH plays an important role in the ammonia oxidation reaction since it improved the power density by a factor of two. Among the PtRh/C electrocatalysts the electrode with Pt:Rh atomic ratio of 90:10 showed the best catalytic activity in electrochemical experiments. In terms of DAFC performance the highest power density and cell potential were obtained using this material for all NH_4OH/KOH concentrations, showing highest power density when using $3\,mol\,L^{-1}$ KOH and $3\,mol\,L^{-1}$ NH_4OH. This power density was almost 60% higher than that obtained with pure Pt electrode. Three effects were identified to contribute to the high performance of the material: (i) improved nitrogen oxide conversion properties on rhodium-based metal; (ii) electronic effect due to a PtRh alloy formation, lowering the adsorption strength of poisonous intermediates and (iii) a synergic effect between Pt and Rh at this composition.

Acknowledgements

The authors wish to thank Laboratório de Microscopia do Centro de Ciências e Tecnologia de Materiais (CCTM) by TEM measurements, FAPESP (2013/01577-0, 2011/18246-0, 2012/22731-4, 2012/03516-5), INCT, Energia e meio ambiente (573783/2008-0) and CNPq (474913/2012-0, 150639/2013-9, 141469/2013-7, 406612/2013-7) for the financial support.

References

[1] C. Zamfirescu, I. Dincer, Fuel Process. Technol. 90 (2009) 729–737.
[2] N. Maffei, L. Pelletier, A. McFarlan, J. Power Sources 175 (2008) 221–225.
[3] J.C. Ganley, J. Power Sources 178 (2008) 44–47.
[4] S.A. Hajimolana, M.A. Hussain, W.M.A.W. Daud, M.H. Chakrabarti, Chem. Eng. Res. Des. 90 (2012) 1871–1882.
[5] R. Lan, J.T.S. Irvine, S. Tao, Int. J. Hydrogen Energy 37 (2012) 1482–1494.
[6] A.A. Boretti, Int. J. Hydrogen Energy 37 (2012) 7869–7876.
[7] S. Appari, V.M. Janardhanan, S. Jayanti, L. Maier, S. Tischer, O. Deutschmann, Chem. Eng. Sci. 66 (2011) 5184–5191.
[8] A. Allagui, M. Oudah, X. Tuaev, S. Ntais, F. Almomani, E.A. Baranova, Int. J. Hydrogen Energy 38 (2013) 2455–2463.
[9] M. Altomare, E. Selli, Catal. Today 209 (2013) 127–133.
[10] M. Kaneko, N. Gokan, N. Katakura, Y. Takei, M. Hoshino, Chem. Commun. 12 (2005) 1625–1627.
[11] K. Yao, Y.F. Cheng, J. Power Sources 173 (2007) 96–101.
[12] C.-M. Hung, Powder Technol. 232 (2012) 18–23.
[13] M.H.M.T. Assumpção, S.G. da Silva, R.F.B. de Souza, G.S. Buzzo, E.V. Spinacé, A.O. Neto, J.C.M. Silva, Int. J. Hydrogen Energy 39 (2014) 5148–5152.
[14] L. Zhou, Y.F. Cheng, Int. J. Hydrogen Energy 33 (2008) 5897–5904.
[15] T.L. Lomocso, E.A. Baranova, Electrochim. Acta 56 (2011) 8551–8558.
[16] A. Allagui, S. Sarfraz, S. Ntais, F. Al momani, E.A. Baranova, Int. J. Hydrogen Energy 39 (2014) 41–48.
[17] S. Le Vot, L. Roué, D. Bélanger, J. Electroanal. Chem. 691 (2013) 18–27.
[18] F.J. Vidal-Iglesias, J. Solla-Gullón, V. Montiel, J.M. Feliu, A. Aldaz, J. Power Sources 171 (2007) 448–456.
[19] C.-M. Hung, J. Hazard. Mater. 163 (2009) 180–186.
[20] A.C.A. de Vooys, M.T.M. Koper, R.A. van Santen, J.A.R. van Veen, J. Electroanal. Chem. 506 (2001) 127–137.
[21] R.S. Henrique, R.F.B. De Souza, J.C.M. Silva, J.M.S. Ayoub, R.M. Piasentin, M. Linardi, E.V. Spinace, M.C. Santos, A.O. Neto, Int. J. Electrochem. Sci. 7 (2012) 2036–2046.
[22] A.O. Neto, M.M. Tusi, N.S. de Oliveira Polanco, S.G. da Silva, M. Coelho dos Santos, E.V. Spinacé, Int. J. Hydrogen Energy 36 (2011) 10522–10526.
[24] M.H.M.T. Assumpção, S.G. da Silva, R.F.B. De Souza, G.S. Buzzo, E.V. Spinacé, M.C. Santos, A.O. Neto, J.C.M. Silva, J. Power Sources 268 (2014) 129–136.
[25] H. Hou, S. Wang, W. Jin, Q. Jiang, L. Sun, L. Jiang, G. Sun, Int. J. Hydrogen Energy 36 (2011) 5104–5109.
[26] D.A. Cantane, W.F. Ambrosio, M. Chatenet, F.H.B. Lima, J. Electroanal. Chem. 681 (2012) 56–65.
[27] R.M. Modibedi, T. Masombuka, M.K. Mathe, Int. J. Hydrogen Energy 36 (2011) 4664–4672.
[28] H. Wang, Z. Liu, S. Ji, K. Wang, T. Zhou, R. Wang, Electrochim. Acta 108 (2013) 833–840.
[29] J.C.M. Silva, R.F.B. De Souza, M.A. Romano, M. D'Villa-Silva, M.L. Calegaro, P. Hammer, A.O. Neto, M.C. Santos, J. Braz. Chem. Soc. 23 (2012) 1146–1153.
[30] J.C.M. Silva, B. Anea, R.F.B. De Souza, M.H.M.T. Assumpcao, M.L. Calegaro, A.O. Neto, M.C. Santos, J. Braz. Chem. Soc. 24 (2013) 1553–1560.
[31] S.Y. Shen, T.S. Zhao, J.B. Xu, Int. J. Hydrogen Energy 35 (2010) 12911–12917.
[32] M. Li, W.P. Zhou, N.S. Marinkovic, K. Sasaki, R.R. Adzic, Electrochim. Acta 104 (2013) 454–461.
[33] Y.S. Kim, S.H. Nam, H.-S. Shim, H.-J. Ahn, M. Anand, W.B. Kim, Electrochem. Commun. 10 (2008) 1016–1019.
[34] T.S. Almeida, L.M. Palma, P.H. Leonello, C. Morais, K.B. Kokoh, A.R. De Andrade, J. Power Sources 215 (2012) 53–62.
[35] NIST X-ray Photoelctron Spectroscopy Database, A.V. Naumkin, A. Kraut-Vass, S.W. Gaarenstroom, C.J. Powell, NIST Standard Reference Database 20 v. 4.1, htttp://srdata.nist.gov/XPS/.
[36] J.L.G. Fierro, J.M. Palacios, F. Tomas, Surface Interface Anal. 13 (1988) 25–32.
[37] G. Li, L. Jiang, B. Zhang, Q. Jiang, D. s. Su, G. Sun, Int. J. Hydrogen Energy 38 (2013) 12767–12773.
[38] L. Jiang, A. Hsu, D. Chu, R. Chen, Int. J. Hydrogen Energy 35 (2010) 365–372.
[39] L. Ma, D. Chu, R. Chen, Int. J. Hydrogen Energy 37 (2012) 11185–11194.
[40] B.K. Boggs, G.G. Botte, Electrochim. Acta 55 (2010) 5287–5293.
[41] C.A. Kruissink, J. Membr. Sci. 14 (1983) 331–366.
[42] E.H. Yu, K. Scott, R.W. Reeve, J. Appl. Electrochem. 36 (2006) 25–32.
[43] A. Allagui, S. Sarfraz, E.A. Baranova, Electrochim. Acta 110 (2013) 253–259.
[44] C. Zhong, W.B. Hu, Y.F. Cheng, J. Mater. Chem. A 1 (2013) 3216–3238.
[45] S. Suzuki, H. Muroyama, T. Matsui, K. Eguchi, J. Power Sources 208 (2012) 257–262.